Miniaturized Circularly Polarized Doppler Radar for Human Vital Sign Detection

Yuchu He, *Student Member, IEEE*, Changzhan Gu, *Senior Member, IEEE*, Haijiang Ma, *Member, IEEE*, Jiang Zhu, *Senior Member, IEEE*, and George V. Eleftheriades, *Fellow, IEEE*

***Abstract*— In this paper, a miniaturized circularly polarized (CP) continuous wave Doppler radar system operating at 2.4 GHz is presented. The radar front end consists of one left-handed CP (LHCP) antenna and one right-handed CP (RHCP) antenna, which share a single patch antenna aperture. Orthogonal polarization is achieved through a modified ring-shaped quadrature hybrid coupler (QHC), and the resulting isolation between the two CP antennas is better than 30 dB. With 0 dBm input power to the transmitting antenna, the proposed radar system can accurately detect heartbeat and respiration movements of human test subjects under 1 m and over a wide angular range. The single dual CP antenna achieves 280% size reduction compared to a traditional two linear polarization patch antenna array with the same isolation level.**

***Index Terms*— Circular polarization, Doppler radar, patch antenna.**

I. Introduction

SHORT-range radar systems are gaining enormous interest recently because they can be applied to various emerging applications such as healthcare sensors, motion detectors, and automotive collision avoidance radars. Specifically, a short-range radar is attractive for home health monitoring since it can monitor accidental fall down, vital signs, and sleep quality [1]–[13]. The simplest type of short-range radar is a continuous wave (CW) Doppler radar. The radar transceivers usually consist of linearly copolarized transmitting (TX) and receiving (RX) antennas. However, such radar transceivers are vulnerable to interference due to the mutual coupling between the antennas, especially when they are close to each other. Energy coupled from the TX antenna into the RX antenna can dominate the signal reflected from the objects (e.g., human body) at a distance and, thus, reduce the range of radar sensing. To maintain good radar signal-to-noise ratio (SNR), TX and RX antennas are adequately separated in space to meet the isolation requirement for specific remote sensing applications. This leads to a large footprint of an antenna array in a radar system that operates at sub-6 GHz, making it impractical to be integrated into small factor health-tracking devices and consumer electronic devices.

To reduce the footprint, Doppler radars have been extensively studied at higher frequencies, e.g., 24 GHz [7], [8], [11], [13]. Both the antenna size and the spacing shrink with the wavelength. In addition, motions have a greater Doppler shift at higher frequencies, which enables a better detection of weak heartbeat signals. However, there are several disadvantages to operating the radar at higher frequencies: 1) the free space path loss increases with frequency; 2) the circuits are generally less power efficient at higher frequencies; and 3) the fabrication tolerance is much tighter and the cost of fabrication and circuit components is generally higher. In order to compensate the large free space path loss, high gain antennas such as phased arrays [13] are used. However, the size of the phased arrays can be significant and the advantage of having a reduced footprint is comprised. In addition, by using high gain antennas, the radar is sensitive only in a narrow angular range. Beam steering is required to detect over a wide angle, which adds significant complexity and cost to the system.

For a radar that operates at the 2.4 GHz industrial, scientific and medical band, which has the advantage of lower free space path loss and fabrication cost, the footprint can be reduced by having the TX and RX parts share a single antenna aperture as in [6], [14], and [15]. This is achieved by using a circulator to separate the transmit and receive signals. However, the circulators are generally ferrite-based devices with large dimensions, making them not ideal for compact devices. In addition, the isolation between the TX and RX ports is usually limited. High gain antennas such as horns may be needed to improve the SNR for weak heartbeat signals.

In this paper, a miniaturized dual circularly polarized (CP) patch antenna is proposed as the radar front end of a low-power 2.4 GHz CW Doppler radar. TX and RX antennas share a single aperture and the isolation is better than 30 dB. This paper is organized as follows: In Section II, the basic Doppler radar operation principles and the theory of circular polarization-based detection mechanism are discussed. In Section III, the design of the dual CP patch antenna, along with its simulated characteristics, is presented. In Section IV,

Manuscript received January 9, 2019; revised May 2, 2019; accepted June 1, 2019. Date of publication July 16, 2019; date of current version October 29, 2019. This work was supported by the Google Internship Program. *(Corresponding author: Jiang Zhu.)*

Y. He is with Google LLC, Mountain View, CA 94043 USA, and also with the Department of Electrical and Computer Engineering, University of Toronto, Toronto, ON M5S 3H7, Canada (e-mail: yuchu.he@utoronto.ca).

C. Gu is with the Key Laboratory of Ministry of Education of Design and Electromagnetic Compatibility of High Speed Electronic System, Shanghai Jiao Tong University, Shanghai 200240, China (e-mail: changzhan@sjtu.edu.cn).

H. Ma, and J. Zhu are with Google LLC, Mountain View, CA 94043 USA (e-mail: hjma@google.com; jiangzhu@google.com).

G. V. Eleftheriades is with the Department of Electrical and Computer Engineering, University of Toronto, Toronto, ON M5S 3H7, Canada (e-mail: gelefth@waves.utoronto.ca).

Color versions of one or more of the figures in this article are available online at http://ieeexplore.ieee.org.

Digital Object Identifier 10.1109/TAP.2019.2927777

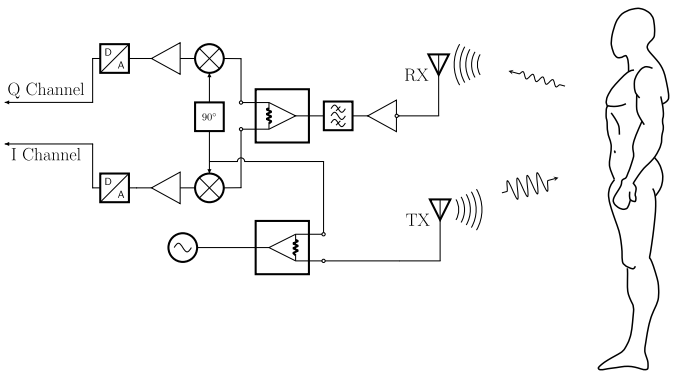

Fig. 1. Single-tone CW Doppler radar system for vital sign detection.

the performance of the proposed CP antenna is simulated with a perfect electric conductor (PEC) as a reflector. For comparison purposes, the simulated results from a conventional linearly polarized (LP) antenna array are also presented. Lastly, the characteristics of the fabricated CP antenna, and the human vital sign measurement results at various distances and angles are shown in Section V.

II. Theory

A. Basic CW Doppler Radar Operation

The basic architecture of a single-tone CW radar for vital sign detection is shown in Fig. 1. The TX antenna sends a single-tone signal, which is reflected off from the human body and captured by the RX antenna. The body movement modulates the reflected signal frequency due to the Doppler effect. By using direct conversion and splitting the received signal into I and Q channels, the baseband signals can be described by the following:

$$I(t) = A \cdot \cos\left[\frac{4\pi}{\lambda}(x(t) + d_0) + \Delta\theta(t)\right] + dc_I \quad (1)$$

$$Q(t) = A \cdot \sin\left[\frac{4\pi}{\lambda}(x(t) + d_0) + \Delta\theta(t)\right] + dc_Q \quad (2)$$

where $\Delta\theta(t)$ is random phase noise; dc_I and dc_Q are the dc bias for the I and Q channels, respectively, d_0 is the nominal distance to the chest; and $x(t)$ is the chest movement, which is assumed to be sinusoidal in the form of $x(t) = A_c \sin(2\pi f_c t)$ [2], [4]. The advantage of splitting the received signal into I and Q channels is that the received signal strength has a strong dependence on the nominal distance d_0. If the signal from one channel is weak, then the signal of the other channel can be strong [4], [16], [17]. As a result, the radar system is more robust. If the random phase noise is very small and can be ignored, and the dc bias is zero, the relative motion can be retrieved using (3). Notice that this method can only retrieve the relative motion $x(t)$ but not that nominal distance d_0

$$x(t) + d_0 = \frac{\lambda}{4\pi} \tan^{-1} \frac{Q(t)}{I(t)}. \quad (3)$$

B. CP Radar Transceiver

Conventional Doppler radars required two separate antennas for the transceiver as shown in Fig. 1. The antennas are linearly copolarized and isolation is poor if they are placed close to each other. The isolation can be improved if the TX and RX signals have orthogonal linear polarizations. However, polarization orthogonality is not desirable in LP radar transceivers as the reflected signal is usually copolarized with the transmit signal. RX with an orthogonal polarization can suffer from a large polarization mismatch. Thus, the TX and RX antennas are usually placed far apart, which leads to a large overall footprint. This size constraint can be overcome with circular polarization. The two separate TX and RX antennas in Fig. 1 can be combined into a single antenna that transmits and receives circular polarizations with opposite handedness, i.e., exciting the TX port of the antenna transmits right-handed circularly polarized (RHCP) and the RX port only receives left-handed circularly polarized (LHCP), or vice versa. By virtue of the TX and RX channels having orthogonal polarizations, the isolation can be very high. Contrary to linear polarization, the CP RX is not mismatched to the reflected signal. This is because circular polarization has a unique property, that is, the handedness of the incident polarization is flipped upon reflection from a metal or dielectric interface (assuming normal incidence) [18]. For example, if the TX sends an RHCP wave, then it reflects from the human abdominal region (assuming the tissues can be modeled as a planar multi-layer lossy dielectric [19]) as an LHCP wave. Consequently, the RX antenna with LHCP receives the reflected signal with no polarization mismatch. Meanwhile, high isolation can be maintained between the TX and RX channels.

III. Dual CP Antenna Design

A dual CP antenna can be created by connecting the dual LP antenna with orthogonal polarizations to a quadrature hybrid coupler (QHC) [20]. The QHC is a four-port microwave device [21] that has an input, an isolation, a through, and a coupled port. With a properly designed QHC, when exciting the input or the isolation port, equal power is delivered to the through and coupled ports with a 90° phase difference. Hence, when the through and coupled ports are used to excite the dual LP patch, CP waves can be generated. This concept has been applied in [11]. However, the QHC is a Lange coupler and it is connected to the patch antenna with edge feed configuration. The coupler is in the same plane as the patch and has a significant footprint. This configuration is acceptable at 24 GHz, but it is not desirable at lower frequencies since the lateral dimension is quite large. In this section, a compact dual CP patch design for 2.4 GHz is presented.

A. Dual LP Patch Design

A dual LP patch antenna is shown in Fig. 2. Two microstrip transmission lines are connected to two vias that are used to excite orthogonal linear polarizations on the patch. The patch is pin fed instead of edge fed because it can be more compact. Otherwise, the QHC has to lie in the same plane with the patch as in [11], resulting to a large lateral footprint. With the pin fed configuration, the QHC can be stacked below the patch to minimize the lateral footprint. In addition, this type of feeding has an additional advantage: the QHC and the feeding lines

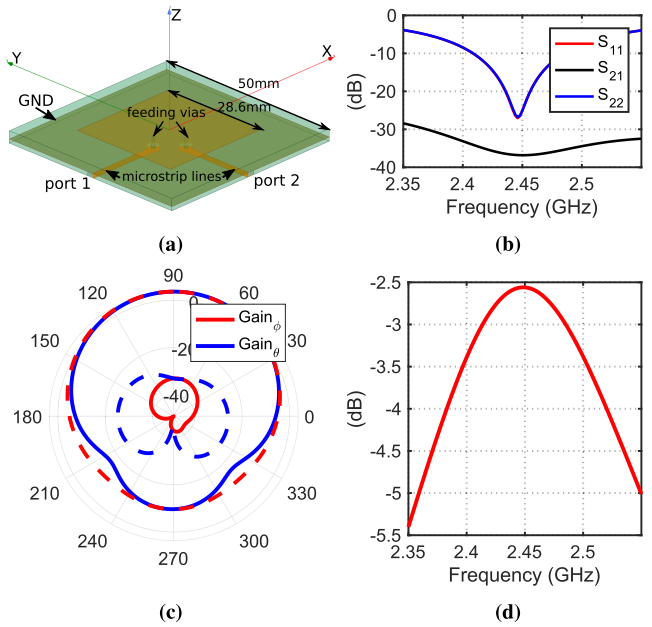

Fig. 2. (a) Geometry of the dual LP square patch. Ports 1 and 2 excite orthogonal linear polarizations. (b) S-parameters of the patch. S_{11} and S_{22} are identical to each other as expected. The isolation is below -35 dB at the target frequency of 2.45 GHz. (c) Radiation pattern in $X-Z$ (solid curves) and $Y-Z$ (dashed curves). $Gain_\theta$ is shown in blue and $Gain_\phi$ is shown in red. (d) Total efficiency, which is calculated by radiated power/input power (1 W). Peak efficiency is -2.6 dB at design frequency.

are shielded by the ground plane; thus, the feeding structures do not affect the polarization purity of the antenna. The overall dimensions of the antenna are 50 mm $\times$ 50 mm $\times$ 3 mm. The substrate is FR4 with a 2 mm thickness between the patch and the ground plane and a 1 mm thickness between the microstrip feed lines and the ground. The patch is a 28.6 mm $\times$ 28.6 mm square.

Since ports 1 and 2 excite orthogonal polarizations, the mutual coupling S_{21} is very small (less than -30 dB) as expected. In addition, the design is symmetric; hence, exciting either ports 1 and 2 (with the other port matched to 50 Ω) leads to identical radiation patterns and antenna efficiencies. These are desirable properties in the CP antenna design.

B. Modified Ring-Shaped Quadrature Hybrid Coupler

The QHC is implemented based on microstrip transmission lines. However, in order to achieve the smallest overall footprint, the conventional rectangular hybrid coupler [21] has been modified as shown in Fig. 3(a). The through and coupled ports (ports 2 and 3) are now inside the coupler structure and can be used to connect to the feeding pins of the patch. As a result, the coupler can be stacked directly below the patch, and the footprint in the lateral direction is minimized. However, due to the sharp bend at the intersection between the rectangular ring and the feed lines of ports 2 and 3, the impedances of those ports are affected. Thus, the minimum isolation between ports 1 and 4 are around -20 dB. To further improve the isolation, the coupler is modified to a ring shape to reduce the sharp bending as shown in Fig. 3(b). The isolation is improved to -30 dB as shown in Fig. 4. In addition, the power difference

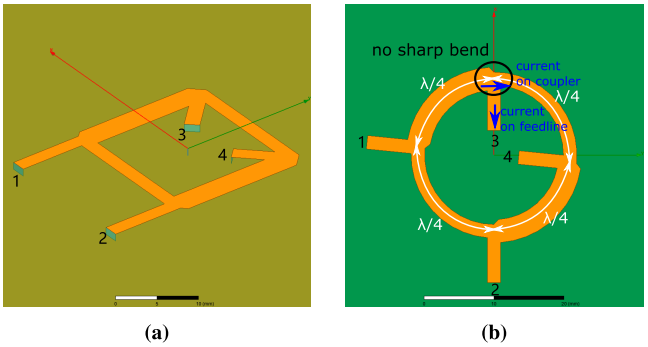

Fig. 3. (a) Conventional rectangular QHC with ports 1–4 as the input, isolation, through, and coupled ports, respectively. Port 1 is the TX port and port 2 is the RX port of the radar. Ports 3 and 4 are connected to the feeding vias of the patch in Fig. 2(a). (b) Ring-shaped QHC. The working principle is exactly the same as the conventional QHC. The quarter-wave transmission lines are curved instead of straight. In this configuration, the sharp bend is eliminated at the junction. In addition, the current following on the feed line and the coupler (shown by the blue arrow) is more orthogonal. This reduces the coupling between the coupler and the feed line, which in turn reduces the impedance mismatch of the feed line and improves return loss and isolation.

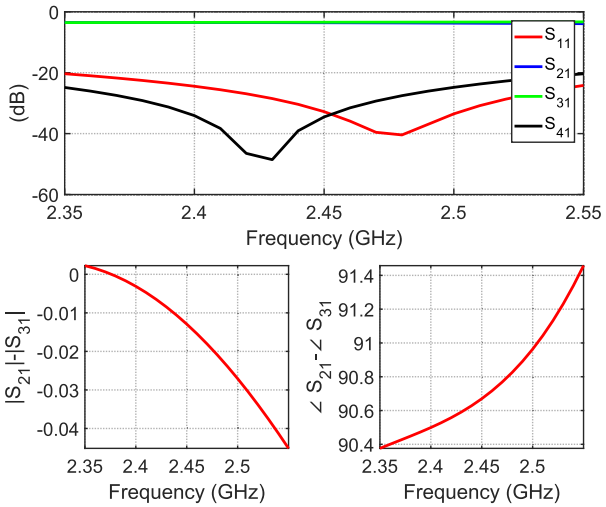

Fig. 4. S-parameters of the ring-shaped QHC. At 2.45 GHz, both the return loss (S_{11}) and the isolation (S_{41}) are around -30 dB. The transmission difference ($|S_{21}|-|S_{31}|$) to the coupled and through ports are very small and the phase difference ($\angle S_{21}-\angle S_{31}$) is almost 90°.

is very small and the phase difference is almost 90° between ports 2 and 3. By combining this modified QHC to the patch presented in Section III-A, a CP patch can be designed with good polarization purity.

C. Dual CP Patch Antenna

By connecting the QHC presented in Section III-B to the dual LP patch in Section III-A, a dual CP patch antenna is designed as shown in Fig. 5. The top layer is the square patch, the middle layer is the ground plane (not shown in the figure), and the bottom layer is the QHC. Ports 1 and 2 of the ring-shaped QHC are the TX and RX ports of the dual CP patch. Ports 3 and 4 are connected to the feeding vias of the patch in Fig. 2(a). By exciting port 1 (TX port), equal power is delivered to ports 3 and 4 with a 90° phase difference.

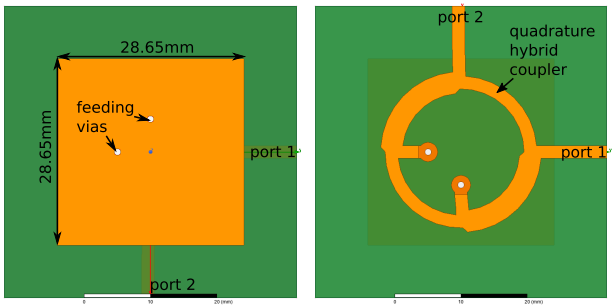

Fig. 5. Patch is fed by the ring-shaped QHC and the lateral footprint is 50 mm × 50 mm. (a) Top view. (b) Bottom view.

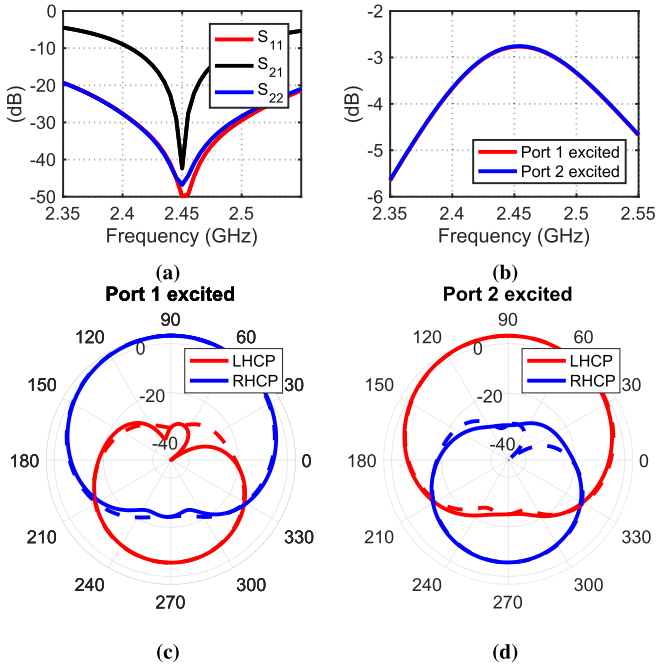

Fig. 6. (a) S-parameters of the CP patch. Both the isolation and the return loss are below −40 dB at 2.45 GHz. (b) Total efficiency. Identical efficiencies were obtained no matter which port is excited. The peak efficiency is about −2.7 dB. The radiation patterns at 2.45 GHz in the XZ (solid lines) and YZ (dashed lines) planes are shown when (c) port 1 is excited and (d) port 2 is excited. When port 1 is excited, an RHCP wave is generated with a gain of 3 dB. The corresponding LHCP component is −32 dB. Similarly, when port 2 is excited, an LHCP wave is generated with a gain of 3 dB. The corresponding RHCP component is −32 dB.

Hence, an RHCP wave can be generated. Similarly, by exciting port 2 (RX port), an LHCP wave can be generated. By the principle or reciprocity, port 2 can be used as the receiving port for an LHCP wave.

The S-parameters are shown in Fig. 6(a). As one can see, both the return losses and the isolation are below −40 dB at the design frequency. The total efficiency and radiation patterns in the XZ and YZ planes are shown in Fig. 6. As expected, identical efficiencies are obtained no matter which port is excited. When port 1 is excited, an RHCP wave is generated with a gain of 3 dB at broadside ($\theta = 90°$). Meanwhile, the gain of the LHCP wave is −32 dB. Thus, extremely high polarization purity is achieved. Similarly, when port 2 is excited, an RHCP wave is generated with high polarization purity.

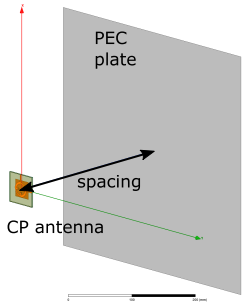

Fig. 7. CP antenna is placed in front of a PEC plate. The transmission between TX and RX (S_{21}) is simulated to verify that CP antenna functions as a proper front end.

IV. Simulations of CP Radar Front End

To verify the concept of using a CP antenna as the radar front end, a simulation is setup as shown in Fig. 7. The proposed CP patch antenna is placed in front of a PEC plate or a multilayer human tissue model. With the addition of the PEC, if the incident CP wave indeed switches to the opposite handedness upon reflection, a change in the transmission (S_{21}) between the TX and RX ports should be observed due to the added reflection from the PEC plate. Furthermore, as the PEC plate moves away from the antenna, S_{21} should decrease due to a larger free space path loss. This is indeed the case as shown in Fig. 8(a). In addition to the monotonic decrease in S_{21}, it also oscillates with respect to the spacing. This is a standing wave pattern formed between the reflected signal and the mutually coupled signal from TX to RX, which interferes constructively or destructively every half a wavelength. The dashed line is the mutual coupling for a standalone antenna in free space, which is established as the noise floor. Since the average signal strength is higher than the noise floor, the SNR is directly improved by the high isolation in the CP antenna. In comparison, S_{21} versus spacing to a PEC plate is shown for a conventional LP patch array in Fig. 8(b). To minimize the footprint, the patches are placed side by side, resulting to a lower isolation ($S_{21} = -21$ dB) for the standalone patch array. As spacing increases, the average S_{21} quickly converges to the noise floor. Thus, from this simulation, it can be seen that the CP antenna not only works as a proper radar front end but also provides better SNR than a conventional LP patch array that is twice the size.

V. Experimental Results

A. Antenna Measurement Results

The fabricated CP patch antenna is shown in Fig. 9(a) and the measured antenna characteristics are shown in Fig. 10. Due to slight inaccuracy in fabricated dimensions and FR4 substrate permittivity, the resonant frequency of the patch is slightly lowered to 2.42 GHz. The return losses are around −20 dB and the isolation between the two ports is −30 dB. The peak total efficiency of the CP patch is −3.3 dB, which

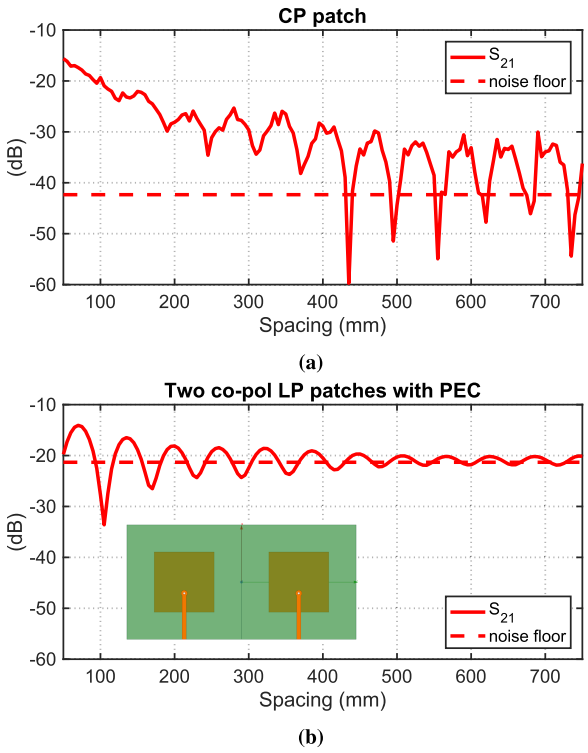

Fig. 8. (a) Simulated S_{21} versus spacing between the antenna and the PEC plate. (b) Simulated S_{21} versus spacing between a conventional LP front end and the PEC plate. The inset in (b) conventional front end, which consists of two LP patches placed side by side. Each patch is 5 cm × 5 cm.

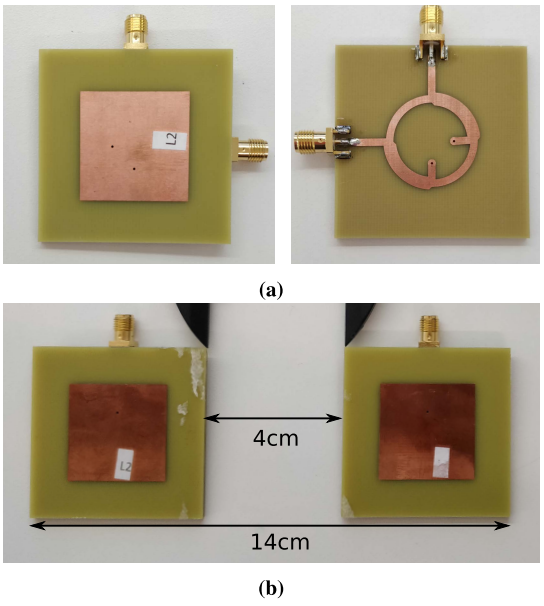

Fig. 9. (a) Top and bottom views of the fabricated CP patch. (b) Conventional LP patch array with equivalent isolation of −30 dB. The spacing between the patches is around 4 cm. The single CP patch has achieved a size reduction of 280%.

is slightly lower than the simulated efficiency of −2.7 dB. The measured radiation patterns in the XZ and YZ planes are shown in Fig. 10(c) and (d). The corresponding axial ratios (ARs) are plotted in Fig. 10(e) and (f). RHCP and LHCP waves are indeed generated by exciting port 1 and port 2, respectively. At broadside ($\theta = 90°$), the gain

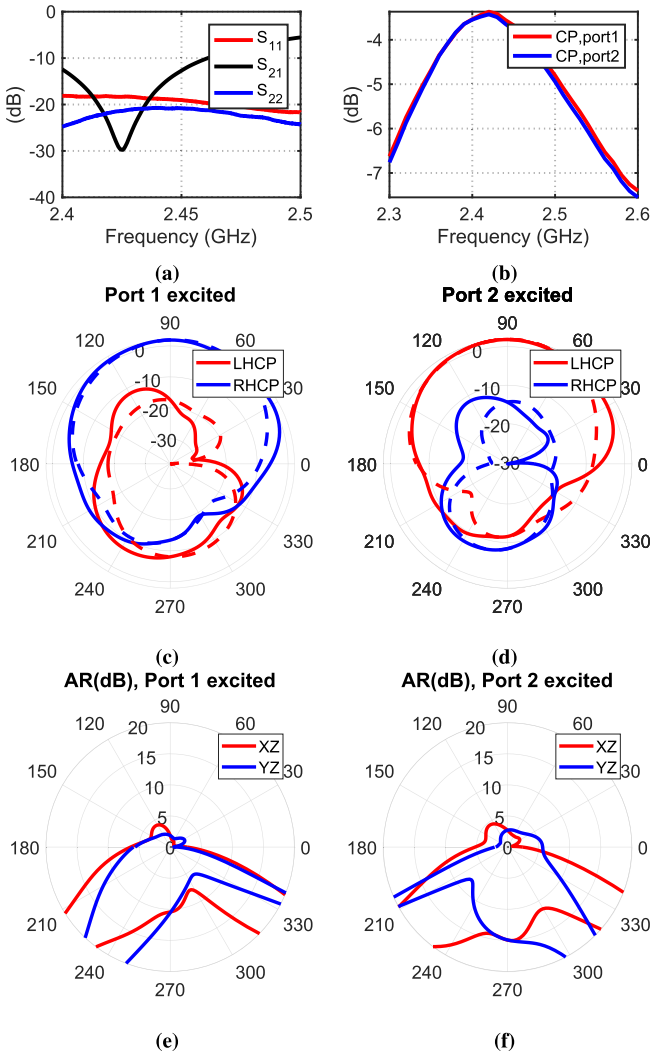

Fig. 10. (a) Measured S-parameters of the fabricated antenna. The return losses for both ports are around −20 dB. The isolation is −30 dB. (b) Measured efficiency of the antenna. The peak efficiency at 2.42 GHz is −3.3 dB. The radiation patterns at 2.42 GHz in the XZ (solid lines) and YZ (dashed lines) planes are shown for (c) port 1 excitation and (d) port 2 excitation. (e) and (f) Corresponding ARs (in dB scale) are plotted. At broadside ($\theta = 90°$), when port 1/2 is excited, LHCP/RHCP wave is generated with a gain of 2 dB, and the corresponding RHCP/LHCP component is −18 dB.

difference between the RHCP and LHCP waves is about −20 dB. The measured polarization purity is not as good as in the simulation. This is because in the simulation, ideal lumped ports are used to excite the antenna, whereas in the measurements, SMA cables are used. Due to the small ground plane of the antenna, a small parasitic current can flow on the SMA cables and radiate, which eventually leads to the deterioration in the polarization purity. This deterioration also leads to a worse AR that is larger than 0 dB (circular polarization has an AR of 0 dB), especially at angles away from broadside. However, as one can see later, the radar can still operate properly even at large angles despite the poor AR. This is because when the antenna transmits RHCP and LHCP waves, both flip their handedness upon reflection. In receive mode, the antenna is sensitive to both RHCP and LHCP waves (due to the poor AR) and can pick up both reflected waves.

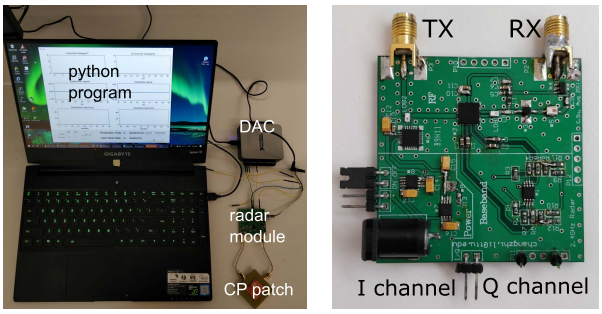

(a) (b)

Fig. 11. (a) CW Doppler radar test system. (b) Radar module circuit board. The output power of TX is 0 dBm. The received signal is down converted to I and Q baseband signals.

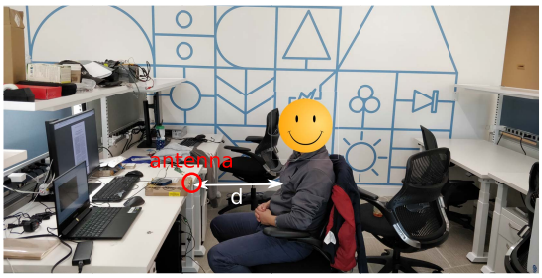

Fig. 12. Human vital sign measurement setup. The broadside of the patch antenna is pointed directly at the chest of the test subject with a spacing of d.

Fig. 9(b) shows the conventional setup with two LP patches as the transmitting and receiving antennas. To achieve a −30 dB isolation, the spacing between the patches is around 4 cm. Thus, the single CP patch has achieved a size reduction of 280%.

B. Radar Measurements

A CW Doppler radar system is shown in Fig. 11. The proposed CP patch antenna is connected to a radar module [22] which outputs 0 dBm power and demodulates the received signal into I and Q baseband signals. A data acquisition card is used to sample the I and Q signals with 12 bit resolution and a python program is used to read the digital data stream, perform some postprocessing, and display the data. The vital sign measurements are performed in a typical office environment with the subject's chest facing the broadside of the patch as shown in Fig. 12. The radar measurement results are compared to ground truth (reference signals) provided by a Vernier respiration belt and a Contec CMS50DA+ photoplethysmography (PPG) finger sensor that obtain accurate respiration and heartbeat data.

Figs. 13–17 show the results measured at various distances d. The original I and Q signals, respiration signals, and heartbeat signals as a function of time are plotted on the left columns of the figures. Since the respiration and heartbeat typically have different frequency ranges, a low-pass filter and a bandpass filter are used to obtain cleaner respiration and heartbeat signals. A fast Fourier transform (FFT) is also performed on the respiration and heartbeat signals, and

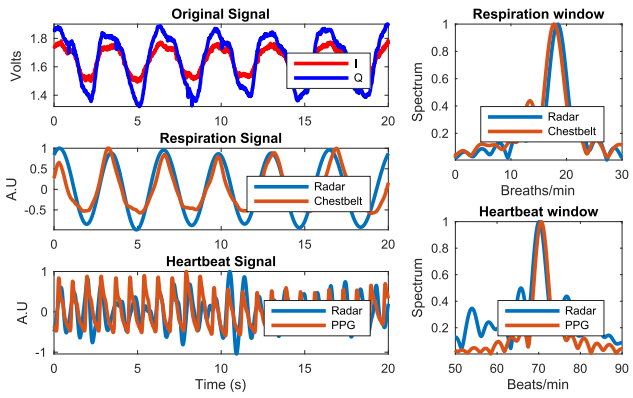

Fig. 13. Vital signs of the test subject are measured at 30 cm.

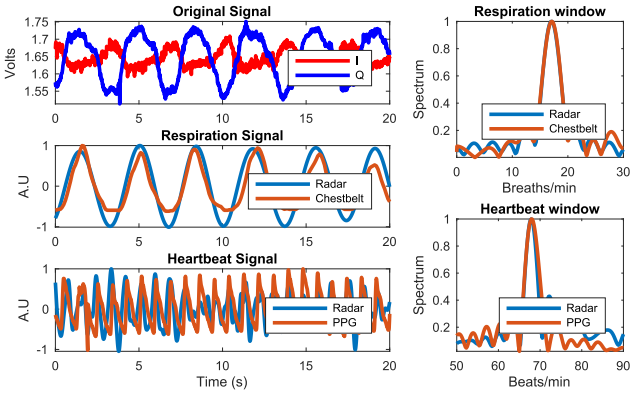

Fig. 14. Vital signs of the test subject are measured at 45 cm.

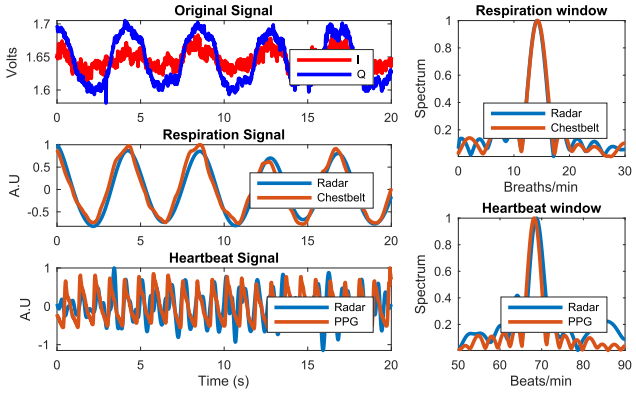

Fig. 15. Vital signs of the test subject are measured at 60 cm.

the frequency responses are plotted on the right columns in Figs. 13–17. In the FFT results, one can find the frequency values (from the horizontal axis) of the peaks, which correspond to the respiration and heartbeat rates. From the time-domain signals, it can be seen that the radar-measured respiration pattern overlaps very well with the respiration belt data even at a distance of 100 cm. The accuracy is also confirmed by the well-aligned frequency peaks (≈18 breaths/min) in the FFT results. From the FFT results of the heartbeat signals, the main peak obtained from the radar signals is well aligned with the peak obtained from

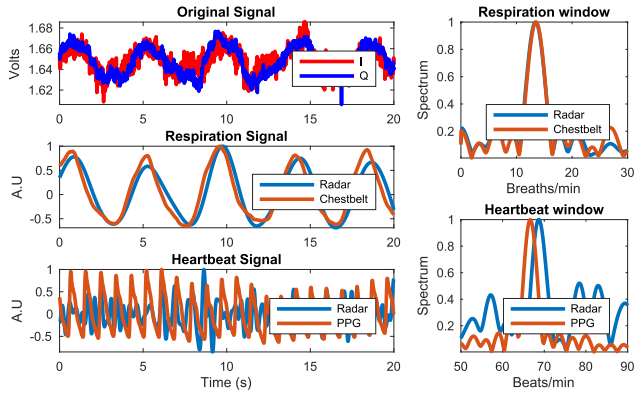

Fig. 16. Vital signs of the test subject are measured at 75 cm.

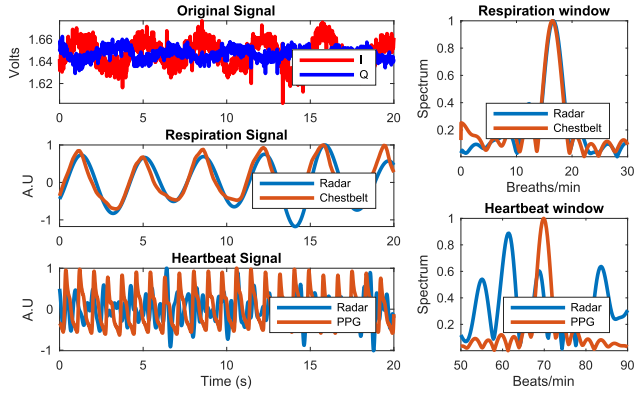

Fig. 17. Vital signs of the test subject are measured at 100 cm.

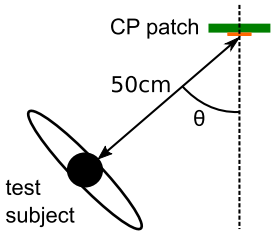

Fig. 18. Illustration of the radar measurements at various angles.

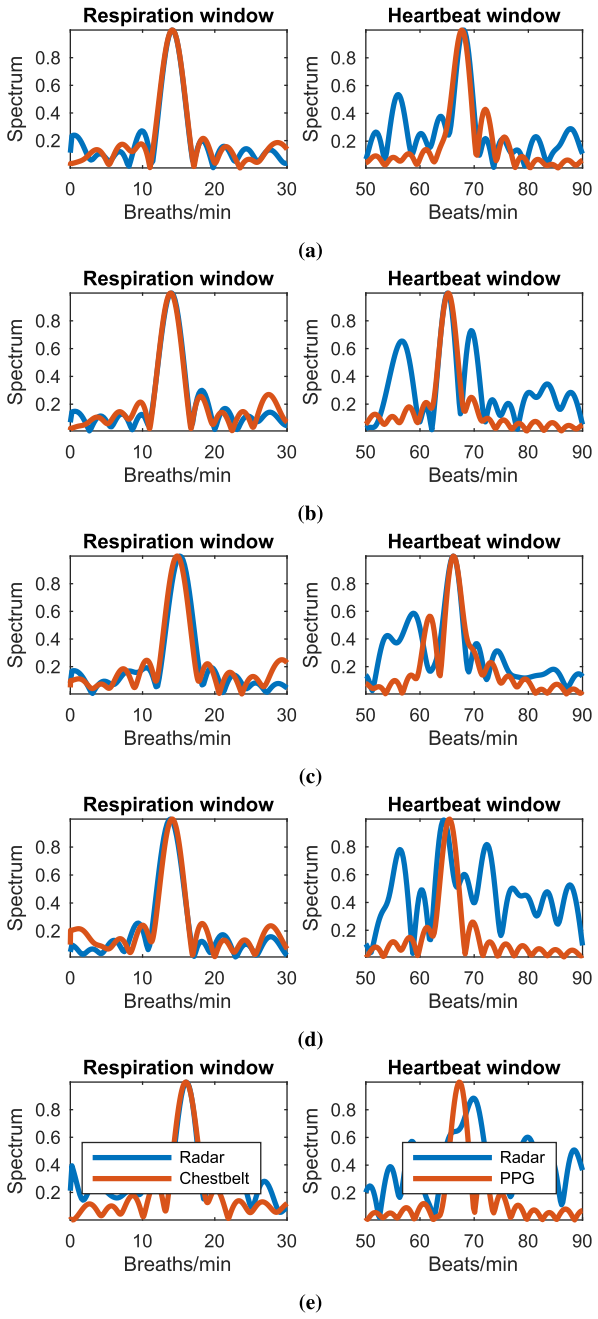

Fig. 19. FFT spectrum of the results measured at (a) $\theta = 0°$, (b) $\theta = 30°$, (c) $\theta = 45°$, (d) $\theta = 60°$, and (e) $\theta = 90°$.

the PPG sensor. However, these peaks start to misalign at 75 cm and 100 cm as shown in Figs. 16 and 17. Thus, the heartbeat, which is a much weaker motion that the respiration, can only be measured accurately up to 60 cm.

The radar is also used to measure the vital signs at various angles as shown in Fig. 18. The test subject's chest is facing toward the antenna with spacing of 50 cm. The vital signs are measured at θ equal to 0°, 30°, 45°, 60°, and 90°. The measured spectrum results are shown in Fig. 19. The radar respiration results correspond very well with chest belt data even at $\theta = 90°$. The heartbeat beat results can be accurate until $\theta = 60°$. Beyond 60°, the antenna gain is 5 dB lower than at broadside. The heartbeat signal strength is approaching the noise floor.

VI. Conclusion

In this paper, a compact dual CP patch antenna with a dimension of 50 mm × 50 mm × 3 mm is proposed as the front end of a CW Doppler radar system. Despite the radar's small footprint, the isolation between the two ports of the CP antenna is better than −30 dB. With this, the CP radar system can accurately detect respiration beyond 1 m and over wide angular range with only 0 dBm output power, while the heartbeat can be accurately detected below 0.5 m within ±45°. It is worth mentioning that the proposed 2.4 GHz radar sensing system allows for its antenna time sharing with Bluetooth and WiFi (2.4 GHz band) radios, opening up a variety of opportunities for its integration with consumer electronic

devices and health-tracking devices where space and size are constrained.

REFERENCES

[1] J. C. Lin, "Noninvasive microwave measurement of respiration," *Proc. IEEE*, vol. 63, no. 10, p. 1530, Oct. 1975.

[2] C. Li, V. M. Lubecke, O. Boric-Lubecke, and J. Lin, "A review on recent advances in Doppler radar sensors for noncontact healthcare monitoring," *IEEE Trans. Microw. Theory Techn.*, vol. 61, no. 5, pp. 2046–2060, May 2013.

[3] C. Li, J. Cummings, J. Lam, E. Graves, and W. Wu, "Radar remote monitoring of vital signs," *IEEE Microw. Mag.*, vol. 10, no. 1, pp. 47–56, Feb. 2009.

[4] C. Gu, "Short-range noncontact sensors for healthcare and other emerging applications: A review," *Sensors*, vol. 16, no. 8, p. 1169, Jul. 2016.

[5] R. Fletcher and J. Han, "Low-cost differential front-end for Doppler radar vital sign monitoring," in *IEEE MTT-S Int. Microw. Symp. Dig.*, Jun. 2009, pp. 1325–1328.

[6] A. Droitcour, V. Lubecke, J. Lin, and O. Boric-Lubecke, "A microwave radio for Doppler radar sensing of vital signs," in *IEEE MTT-S Int. Microw. Symp. Dig.*, vol. 1, May 2001, pp. 175–178.

[7] C. Li, Y. Xiao, and J. Lin, "Experiment and spectral analysis of a low-power Ka-band heartbeat detector measuring from four sides of a human body," *IEEE Trans. Microw. Theory Techn.*, vol. 54, no. 12, pp. 4464–4471, Dec. 2006.

[8] E. F. Greneker, "Radar sensing of heartbeat and respiration at a distance with applications of the technology," in *Proc. Radar Syst.*, Oct. 1997, pp. 150–154.

[9] C. Gu, Z. Peng, and C. Li, "High-precision motion detection using low-complexity Doppler radar with digital post-distortion technique," *IEEE Trans. Microw. Theory Techn.*, vol. 64, no. 3, pp. 961–971, Mar. 2016.

[10] F. Adib, H. Mao, Z. Kabelac, D. Katabi, and R. C. Miller, "Smart homes that monitor breathing and heart rate," in *Proc. 33rd Annu. ACM Conf. Human Factors Comput. Syst.*, New York, NY, USA, Apr. 2015, pp. 837–846. doi: 10.1145/2702123.2702200.

[11] J.-G. Kim, S.-H. Sim, S. Cheon, and S. Hong, "24 GHz circularly polarized Doppler radar with a single antenna," in *Proc. Eur. Microw. Conf.*, vol. 2, Oct. 2005, pp. 1382–1386.

[12] J.-H. Lee, J. M. Hwang, D. H. Choi, and S.-O. Park, "Noninvasive biosignal detection radar system using circular polarization," *IEEE Trans. Inf. Technol. Biomed.*, vol. 13, no. 3, pp. 400–404, May 2009.

[13] T.-W. Hsu and C.-H. Tseng, "Compact 24-GHz Doppler radar module for non-contact human vital-sign detection," in *Proc. Int. Symp. Antennas Propag. (ISAP)*, Okinawa, Japan, Oct. 2016, pp. 994–995.

[14] F.-K. Wang, T.-S. Horng, K.-C. Peng, J.-K. Jau, J.-Y. Li, and C.-C. Chen, "Single-antenna Doppler radars using self and mutual injection locking for vital sign detection with random body movement cancellation," *IEEE Trans. Microw. Theory Techn.*, vol. 59, no. 12, pp. 3577–3587, Dec. 2011.

[15] T.-Y. Chin, K.-Y. Lin, S.-F. Chang, and C.-C. Chang, "A fast clutter cancellation method in quadrature Doppler radar for noncontact vital signal detection," in *IEEE MTT-S Int. Microw. Symp. Dig.*, May 2010, pp. 764–767.

[16] A. D. Droitcour, O. Boric-Lubecke, V. M. Lubecke, J. Lin, and G. T. A. Kovacs, "Range correlation and I/Q performance benefits in single-chip silicon Doppler radars for noncontact cardiopulmonary monitoring," *IEEE Trans. Microw. Theory Techn.*, vol. 52, no. 3, pp. 838–848, Mar. 2004.

[17] Y. Xiao, J. Lin, O. Boric-Lubecke, and M. Lubecke, "Frequency-tuning technique for remote detection of heartbeat and respiration using low-power double-sideband transmission in the ka-band," *IEEE Trans. Microw. Theory Techn.*, vol. 54, no. 5, pp. 2023–2032, May 2006.

[18] C. A. Balanis, *Advanced Engineering Electromagnetics*, 2nd ed. Hoboken, NJ, USA: Wiley, 2012.

[19] C. Gabriel, "Compilation of the dielectric properties of body tissues at RF and microwave frequencies," Dept Phys., King's Coll, London, U.K., Tech. Rep. AL/OE-TR-199-0004, 1996.

[20] C. Balanis, *Antenna Theory and Design*. Hoboken, NJ, USA: Wiley, 2005.

[21] D. M. Pozar, *Microwave Engineering*. Hoboken, NJ, USA: Wiley, 2009.

[22] C. Gu and C. Li, "From tumor targeting to speech monitoring: Accurate respiratory monitoring using medical continuous-wave radar sensors," *IEEE Microw. Mag.*, vol. 15, no. 4, pp. 66–76, Jun. 2014.

Yuchu He (S'15) received the B.A.Sc. degree in engineering science and the M.A.Sc. degree in electrical engineering from the University of Toronto, Toronto, ON, Canada, in 2010 and 2013, respectively, where he is currently pursuing the Ph.D. degree.

His current research interests include infrared metamaterial devices, low mutual-coupling MIMO antennas, low loss and low mismatch graded-index dielectric lenses, and novel metamaterial impedance matching layers and radomes for millimeter-wave applications.

Changzhan Gu (S'07–M'13–SM'18) received the B.S. and M.S. degrees from Zhejiang University, Hangzhou, China, in 2006 and 2008, respectively, the M.S. degree from the University of Florida, Gainesville, FL, USA, where he attended the Ph.D. Program, in 2010, and the Ph.D. degree in electrical engineering from Texas Tech University, Lubbock, TX, USA, in 2013.

He was with Google, Mountain View, CA, USA, where he was involved in the Project Soli with Google Advanced Technology and Projects (ATAP) and consumer hardware products at Google Hardware. He is currently an Associate Professor with Shanghai Jiao Tong University (SJTU), Shanghai, China.

Dr. Gu is a member of the Technical Committee of IEEE MTT-S TC10. He served as a TPRC/TPC Member for several conferences such as IMS2018/2019. He was a recipient of the Best/Excellent Paper Awards from IEEE Conferences as an author/coauthor (seven times), the 2012 Chinese Government Award for Outstanding Self-Financed Students Abroad, and the Texas Tech Horn Professors Graduate Achievement Award in 2013. He received the IEEE Microwave Theory and Techniques Society (MTT-S) Graduate Fellowship in 2013. He is an Associate Editor for the IEEE TRANSACTIONS ON BIOMEDICAL CIRCUITS AND SYSTEMS (TBioCAS) and *IET Microwave, Antenna and Propagation* (MAP). He was an Area Editor for *International Journal of Electronics and Communications* from 2014 to 2016.

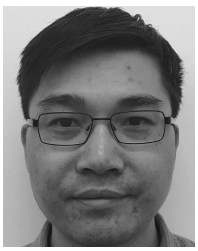

Haijiang Ma (S'10–M'18) received the B.S. and M.S. degrees in electrical engineering from Zhejiang University, Hangzhou, China, in 2004 and 2006, respectively, and the Ph.D. degree in electrical engineering from the University of Illinois, Chicago, IL, USA, in 2012.

Prior to Google and MaxLinear, Inc., San Jose, CA, USA, he was with Teradyne, Inc., North Reading, MA, USA, where he was involved in signal/power integrity and high-speed digital design for semiconductor automatic test equipment test systems. He was with MaxLinear, Inc., where he was involved in microwave/millimeter-wave transceiver systems and high-speed electrical/optical interfaces solutions for broadband and high-speed wireless (5G) and wired networking infrastructures. In 2015, he joined Google, Mountain View, CA, USA, where he developed antennas and RF systems on various best-selling consumer wireless electronic products powered by Google AI for smart-home applications. His current research interests include miniaturized antennas and RF/microwave circuits, MIMO, compact wireless systems, radar, wireless sensing, and advanced high-frequency/speed electronic systems.

Jiang Zhu (S'04–M'10–SM'15) received the B.S. degree in electrical engineering from Zhejiang University, Hangzhou, China, in 2003, the M.A.Sc. degree in electrical engineering from McMaster University, Hamilton, ON, Canada, in 2006, and the Ph.D. degree in electrical engineering from the University of Toronto, Toronto, ON, Canada, in 2010.

From 2010 to 2014, he was a Senior Antenna Engineer with Apple Inc., Cupertino, CA, USA. From 2014 to 2016, he was a Founding Member of Verily Life Science, South San Francisco, CA, USA, a subsidiary of Alphabet Inc. He is currently a Technical Lead Manager with Google LLC, Mountain View, CA, USA, and leads Antenna and RF Research and Development for Emerging Wearables, Virtual Reality and Augment Reality projects and technologies. He has authored or coauthored scientific results in *Physical Review Letters*, the IEEE TRANSACTION ON ANTENNAS AND PROPAGATION, the IEEE TRANSACTION ON MICROWAVE THEORY AND TECHNIQUES, IEEE ANTENNAS AND WIRELESS PROPAGATION LETTERS, and *IET Microwaves, Antennas and Propagation, and Electronic Letters*. He holds 48 granted/filed patents. His current research interests include mobile antennas, wearables/healthcare, RF sensing, and metamaterials.

Dr. Zhu is a member of Industrial Initiatives and Listings for the IEEE Antennas and Propagation Society. He serves on TPC and TPRC for numerous conferences, including IEEE APS, IMS, and RWS. He was the recipient of the IEEE Antennas and Propagation Society Doctoral Research Award in 2009. He has been an Associate Editor for the IEEE TRANSACTION ON ANTENNAS AND PROPAGATION, IEEE ANTENNAS AND WIRELESS PROPAGATION LETTERS, and *IET Microwaves, Antennas and Propagation*.

George V. Eleftheriades (S'86–M'88–SM'02–F'06) received the M.S.E.E. and Ph.D. degrees in electrical engineering from the University of Michigan, Ann Arbor, MI, USA, in 1989 and 1993, respectively.

From 1994 to 1997, he was with the Swiss Federal Institute of Technology, Lausanne, Switzerland. He is currently a Professor with the Department of Electrical and Computer Engineering, University of Toronto, Toronto, ON, Canada, where he holds the Canada Research/Velma M. Rogers Graham Chair in nano- and micro-structured electromagnetic materials. He is a recognized international authority and pioneer in the area of metamaterials. He leads a group of 12 graduate students and researchers in the areas of electromagnetic and optical metamaterials, and metasurfaces, antennas and components for broadband wireless communications, novel antenna beam-steering techniques, far-field super-resolution imaging, radars, plasmonic and nanoscale optical components, and fundamental electromagnetic theory. His current research interests include demonstrating the unique electromagnetic properties of metamaterials, used in lenses, antennas, and other microwave and optical components to drive innovation in fields such as satellite communications, defense, medical imaging, microscopy, automotive radar, and wireless telecommunications.

Dr. Eleftheriades served as a member for the IEEE AP-Society Administrative Committee (AdCom) from 2007 to 2012. In 2009, he was elected as a fellow of the Royal Society of Canada. Papers that he coauthored have received numerous awards such as the 2009 Best Paper Award from IEEE MICROWAVE AND WIRELESS PROPAGATION LETTERS, the R. W. P. King Best Paper Award (twice) from the IEEE TRANSACTIONS ON ANTENNAS AND PROPAGATION in 2008 and 2012, and the 2014 Piergiorgio Uslenghi Best Paper Award from IEEE ANTENNAS AND WIRELESS PROPAGATION LETTERS. He was a recipient of the Ontario Premier's Research Excellence Award in 2001, the University of Toronto's Gordon Slemon Award in 2001, the E.W.R. Steacie Fellowship from the Natural Sciences and Engineering Research Council of Canada in 2004, the 2008 IEEE Kiyo Tomiyasu Technical Field Award, and the 2015 IEEE AP-S John Kraus Antenna Award. He served as an Associate Editor for the IEEE TRANSACTIONS ON ANTENNAS AND PROPAGATION (AP). He was an IEEE AP-S Distinguished Lecturer from 2004 to 2009. He served as the General Chair for the 2010 IEEE International Symposium on Antennas and Propagation held in Toronto, ON, Canada.